How Can New Imaging Modalities Help in the Practice of Radiology?

Yeni Görüntüleme Yöntemleri Radyoloji Pratiğine Nasıl Yardım Eder?

Berhan Pirimoglu, Recep Sade, Hayri Ogul, Mecit Kantarci, Suat Eren, Akın Levent

ABSTRACT

The purpose of this article was to provide an up-to-date review on the spectrum of new imaging applications in the practice of radiology. New imaging techniques have been developed with the objective of obtaining structural and functional analyses of different body systems. Recently, new imaging modalities have aroused the interest of many researchers who are studying the applicability of these modalities in the evaluation of different organs and diseases. In this review article, we present the efficiency and utilization of current imaging modalities in daily radiological practice.

Keywords: Imaging, MRI, CT, ultrasound, new techniques.

ÖZ

Bu çalışmanın amacı radyoloji pratiğinde yeni görüntüleme uygulamalarını içeren bir spektrumu derleme şeklinde sunmaktır. Yeni görüntüleme teknikleri vücuttaki farklı sistemlerin yapısal ve fonksiyonel analizleri ile elde edilerek geliştirilmiştir. Son yıllarda, farklı organ ve hastalıkların değerlendirilmesinde birçok araştırmacı yeni görüntüleme modaliteleri üzerine yoğunlaşmaktadır. Bu derleme çalışmada, biz günlük radyoloji pratiğinde güncel görüntüleme tekniklerinin etkinliği ve kullanımını sunduk.

Anahtar Kelimeler: Görüntüleme, MR, BT, ultrasonografi, yeni

Introduction

Radiological imaging techniques encompass techniques that could be performed to evaluate a patient. Physicians and radiologists should be familiar with the advantages of new imaging modalities [1]. Advanced imaging techniques have permitted the meaningful acquiring of images with higher accuracy [2]. The ensuing review article presents the use of these new imaging modalities in neuroradiology, abdomen imaging, musculoskeletal imaging, interventional radiology breast imaging, pediatric radiology, and other radiological procedures.

1. Neuroimaging

1.1. Brain Perfusion Imaging

Perfusion MRI techniques are advanced methods that reveal information unavailable in conventional MRI. In particular, these techniques have numerous applications with regard to the characterization of tumors (Figure 1) [3]. Perfusion imaging techniques also reveal information on the hemodynamic state of the brain tissue. Concordantly, they reveal details about hypoperfused areas [4, 5].

Arterial spin labeling (ASL) was developed in the 2000s [6]. It does not involve any contrast agent. Because of nephrogenic systemic fibrosis, perfusion imaging in patients with renal deficiency has induced massive alarm in radiologists. If a contrast agent is not required, ASL escapes a potential needle rod in the pediatric population [7-9].

Perfusion imaging accessible is quantitative presenting changes in cerebral blood volume, cerebral blood flow, and mean transit time. Dynamic contrast-enhanced perfusion applications are first-pass methods that are T2- or T2*-weighted sequences. The regional evaluations of a cerebral perfusion reveal, for simple assessment, the therapy, ischemic stroke evaluation, and brain tumors [10-12]. CT perfusion imaging was first performed in 1980. As CT involves ion-

Department of Radiology, Ataturk University School of Medicine, Erzurum, Turkey

Received: November 16, 2016
Accepted: December 7, 2016

Correspondence to: Berhan Pirimoglu
Department of Radiology, Atatürk University School of Medicine, Erzurum, Turkey
E-mail: berhan.dr@gmail.com

DOI 10.5152/eajm.2016.0260

izing radiation, MRI may be preferred in daily practice [13, 14].

1.2. Diffusion-weighted Imaging

Diffusion-weighted imaging (DWI) is based on the principle of mobile molecules. Mobile molecules undergo a substantial loss of signals that are related to the diffusion coefficient, as well as sequence parameters chosen by different b-values [15]. The apparent diffusion coefficient (ADC) corresponds to microscopic water diffusion characteristics. DWI can reveal the cellularity of tumors because cells represent a barrier to water diffusion [3, 4]. Diffusion kurtosis imaging is an attempt to account for this variation, to reveal a more accurate model of diffusion, and to capture non-Gaussian diffusion. It can evaluate whether the variant distribution pattern can reveal important microstructural information about the brain and improve white matter characterization. Important imaging features for assessing disease progression and treatment responses can be determined via diffusion kurtosis imaging [16].

1.3. Diffusion Tensor Imaging (DTI) and Functional Brain Imaging

Diffusion tensor MRI is a method that has been advanced more recently than the isotropic diffusion technique. It can be utilized in some disorders because normal brain white matter is extremely integrated [15]. Diffusion tensor MRI reveals a good design for determining changes in the integrity of white matter structures. White matter disorders can be detected by DTI studies that are not evident on conventional MRI examinations. It is a good application for evaluating guidance in preoperatively detecting white matter tracts (Figure 2) [17]. Functional magnetic resonance (MR) imaging has been used in many studies to better understand how a healthy brain works [18, 19].

1.4. Proton MR Spectroscopy

There are some important diagnostic challenges in the differentiation of benign neoplasms from malignant neoplasms, cystic neoplasms from brain abscess, and tumor recurrence from radiation-induced necrosis. Proton MR spectroscopy (MRS) can reveal knowledge methods or stimulated-echo acquisition mode or point-resolved excitation spin-echo. Important metabolites detected by MRS involve N-acetyl aspartate (NAA), creatine, choline, lactate, myoinositol, and lipids. As soon as the delivery of oxygen and nutrients ceases, anaerobic glycolysis takes over. Lactate is easily determined by its characteristic doublet appearance at 1.3 ppm. A high peak of choline is seen in both intra-axial and extra-axial tumors (Figure 3). A high choline peak, however, is not confined to neoplastic conditions and can be seen in other diseases, for example, in tumefactive multiple sclerosis. The lactate peak and mobile lipid peaks are seen in more malignant tumors and in tumors with necrosis. Radiation necrosis produces a rather flat spectrum because of a reduction in the amount of NAA and choline. Lactate may be seen [20-23].

1.5. Susceptibility-weighted Imaging

Susceptibility-weighted imaging (SWI) is sensitive to compositions that distort the local magnetic competition and make it available in determining hemorrhages and calcium deposits. The most common use of SWI is in the detection of small amounts of hemorrhage or calcium deposits that may be absent on MRI examinations. Phase images could be available in measuring iron content and other substances that change the local field. The development of SWI has opened the door to upgraded contrast and upgraded the determination of hemorrhage in tumors [24, 25].

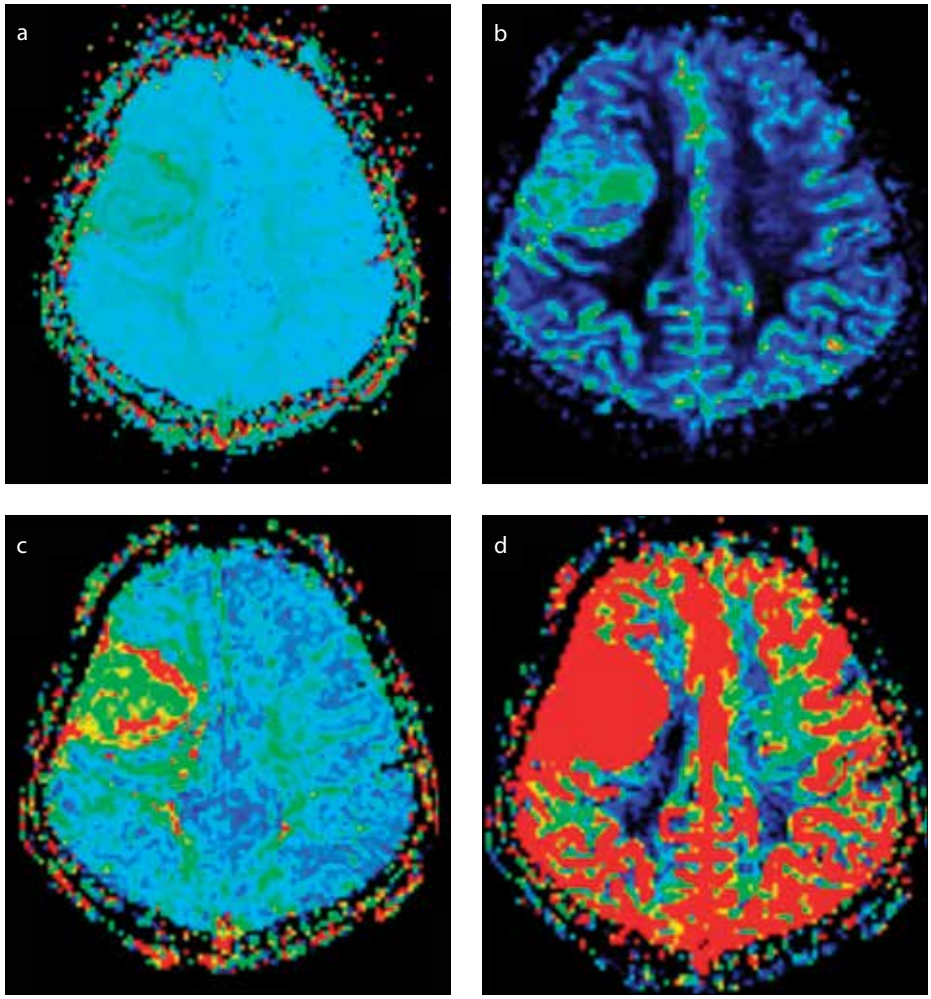

Figure 1. a–d. A meningioma is located at the right cerebral hemisphere: (a) moderately high TTP, (b) significantly high CBF, (c) high MTT, and (d) significantly high CBV
TTP: time to peak; CBF: cerebral blood flow; MTT: cerebral blood volume

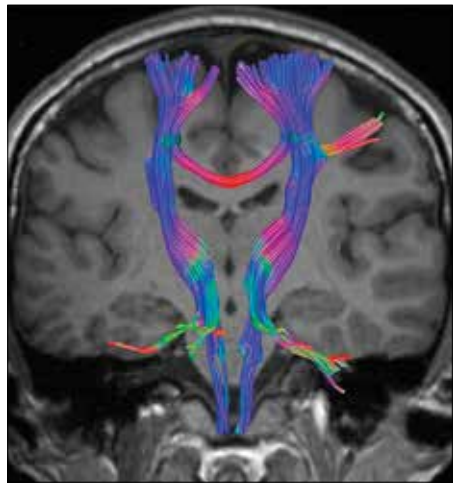

Figure 2. DTI shows bilateral corticospinal tracts and anterior commissural tracts.
DTI: diffusion tensor imaging

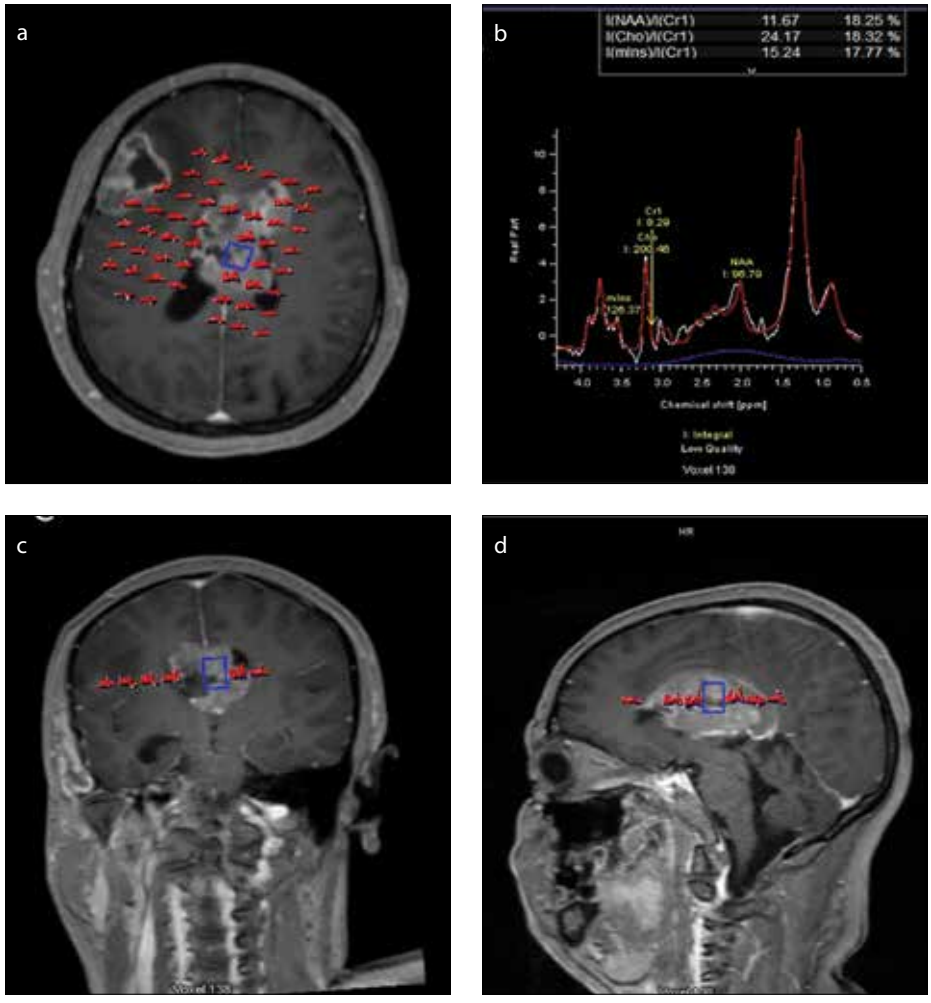

Figure 3. a–d. A multivoxel with short TE (TE: 35 ms) MR spectroscopy image from a glial tumor (a, c, and d) shows elevated lactate levels, lipid peaks, and Cho/NAA ratio (b).

1.6. Cerebrospinal Fluid Flow MRI

Cerebrospinal fluid (CSF) areas involve ventricles and subarachnoid spaces. CSF motion is a combined effect of the CSF production rate and superposed cardiac pulsations. The most common technique used is time-resolved 2D phase-contrast MRI (Figure 4). A typical CSF flow value is 5–8 cm/s. In patients with hyperdynamic circulation, much higher CSF flow values of up to 25 cm/s can be seen [26].

2. Abdomen Imaging

2.1. Ultrasound Elastography

Ultrasound (US) elastography is performed with the transmission of a pulse to the surface of the area of interest. A newer US elastography technique called acoustic radiation force impulse has recently been developed within a regular ultrasonography device (Figure 5). It differs from past elastography systems, which perform a pressure manually to the surface of the organ or a mechanical vibration to induce an elastic shear wave with only M-mode US imaging. It is the simple relationship between palpation and elastography that calls for many applications of this palpation imaging such as breast tumor characterization and hepatic fibrosis staging [27-29].

2.2. Contrast-enhanced Ultrasonography

US contrast agents are often gas-filled microbubbles. These contrast materials have been developed for enhancing B-mode and Doppler US examinations. The effect of US contrast agents is principally due to increased backscattering compared with that from blood and former structures. Using the color Doppler technique, US contrast agents enhance the frequency or power intensity, giving rise to stronger color encodings. During the vascular phase, in patients with hemangiomas, hepatocellular carcinoma and metastasis have revealed that the use of the harmonic mode with US contrast agents can renovate the characterization of these lesions [30-32].

2.3. Dual Energy CT Imaging

Dual energy CT imaging is a recent method that differentiates tissues and relies on CT density

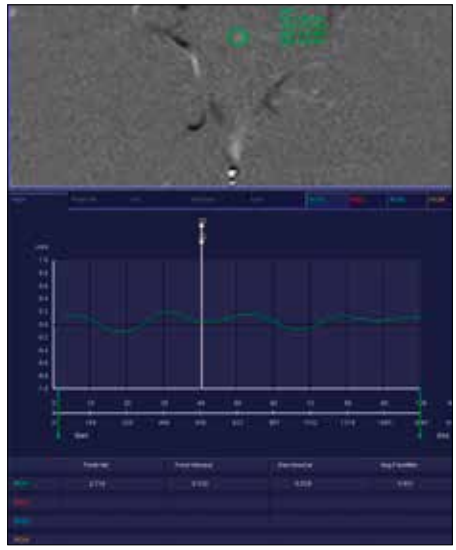

Figure 4. BOS flow MRI shows quantitative flow measurement at the aqueduct of the sylvius.

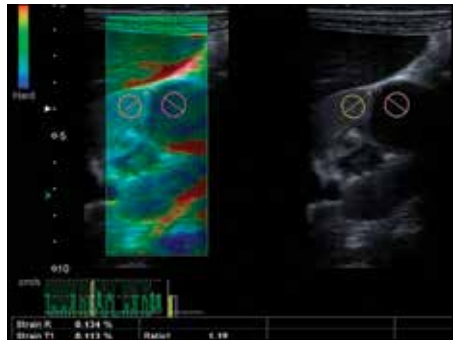

Figure 5. An elastography image shows a lymphoma located at the upper lobe of the right kidney. The lesion strain value is 0.113%.

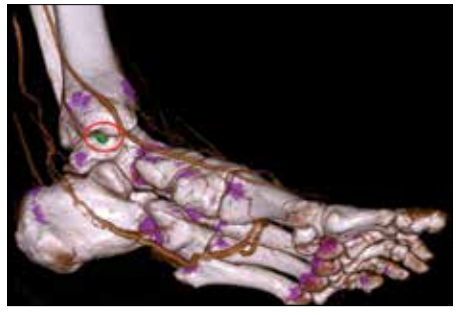

Figure 6. 3D dual energy BT shows a monosodium urate monohydrate crystal (red circle).

treasures obtained from two simultaneous CT acquisitions at different tube potentials. Tube currents that are 80 and 140 kVp are commonly used as these lead to maximum density differences between different organs. Potential clinical applications include the evaluation of liver masses, gout, and pancreatic and bowel diseases (Figure 6) [2, 33-35].

2.4. CT Perfusion Imaging

CT perfusion imaging is a recently developed method for quantitatively assessing tissue blood

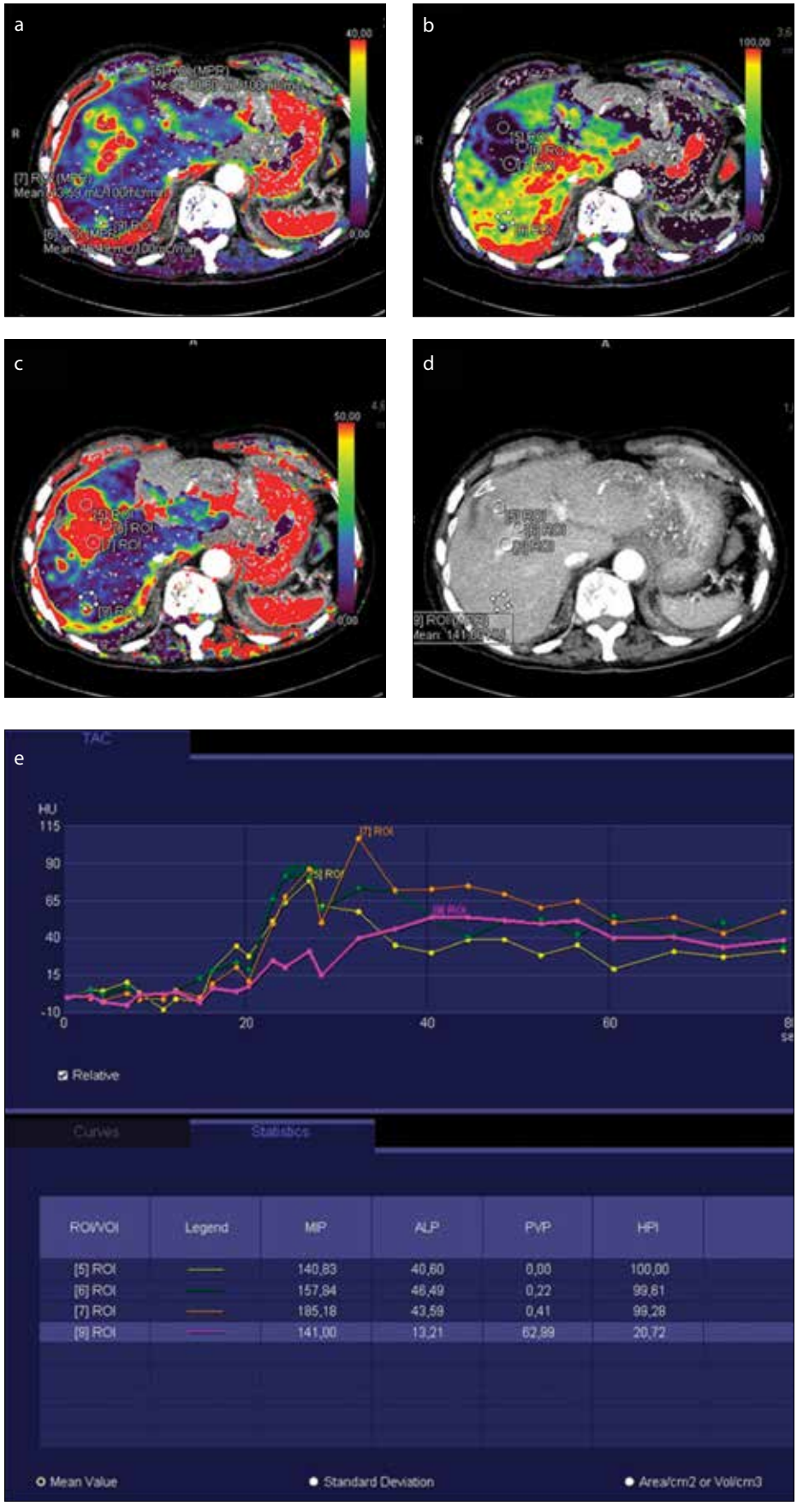

Figure 7. a–e. There is an HCC lesion located at segment V in the liver. (a-d) CT perfusion characteristics. (e) the perfusion graphics of these lesions.
CT: computed tomography; HCC: Hepatocellular carcinoma

features. Hepatic CT perfusion imaging enables the analysis of liver function and the measurement of the following: tissue blood flow (BF, mL/min/100 g) and tissue blood volume (BV; mL/100 g). CT perfusion imaging is becoming a preferred functional tool in the field of oncology, and it has the potential to play a crucial role in the management of oncological procedures. The perfusion parameters of hepatocellular carcinoma can be separated from background liver parenchyma. Hepatocellular carcinoma has higher BF and BV than the background liver levels. CT perfusion is a recently reveals for quantitative evaluation of hemodynamic changes in tissue (Figure 7) [36-39].

2.5. Advanced Diffusion-Weighted and MR Perfusion Imaging in the Abdomen

Diffusion-weighted imaging is increasingly performed in the abdomen for obtaining results, particularly in the assessment of diffuse and focal liver disorders. Restricted diffusion in a mass determines the higher signal intensity on diffusion images and corresponding lower ADC values. The echo-planar method is most frequently used in combination with fat suppression in the abdomen. Neoplasms show restricted diffusion on higher b-value (≥400–500 s/mm^2) images and correspondingly lower ADC values. Intravoxel incoherent motion created with the use of different b-values is a promising technique for the differentiation between benign and malignant liver masses (Figure 8) [40-43].

Perfusion-weighted MRI is a technique for evaluating perfusion characteristics in liver masses. It yields a consider between spatial resolution and temporal resolution. We offer the utilization of 10 mL of intravenous contrast agent followed by 20 mL saline, with injection order of 3–5 ml/s. Perfusion-weighted MRI is a good technique for detecting the fibrosis, cirrhosis, and angiogenesis features of hepatocellular carcinoma. K-trans is a measure of capillary permeability obtained using dynamic contrast-enhanced perfusion MRI. It is calculated by measuring the accumulation of contrast material in the extravascular space [44, 45].

2.6. Hepatocyte-specific Contrast Agents

Contrast-enhanced MR cholangiography using hepatobiliary contrast agents, such as gadobenate dimeglumin (Gd-BOPTA) and gadolinium ethoxybenzyl diethylenetriamine pentaacetic acid (Gd-EOB-DTPA), has emerged in the last decade as a technique to image the biliary tree due to its capability of visualizing biliary complications. Approximately 3e5% of the injected dose of Gd-BOPTA and 50% of Gd-EOB-DTPA are excreted in the human biliary system. Therefore, Gd-EOB-DTPA may provide adequate biliary

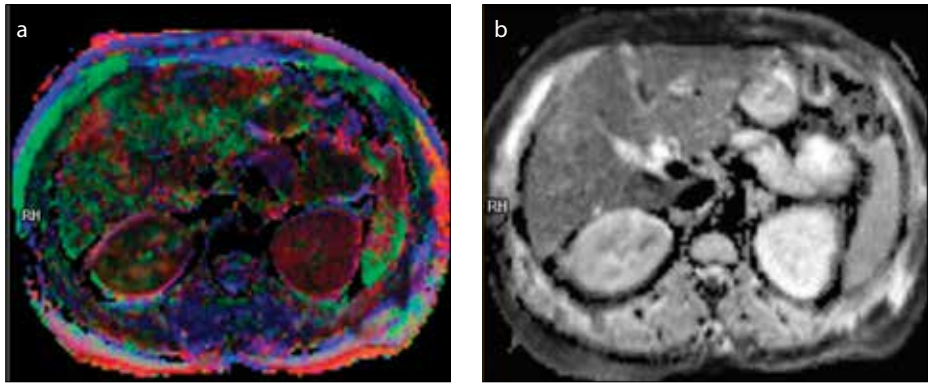

Figure 8. a, b. (a) IVIM diffusion image. (b) IVIM ADC map.
ADC: apparent diffusion coefficient

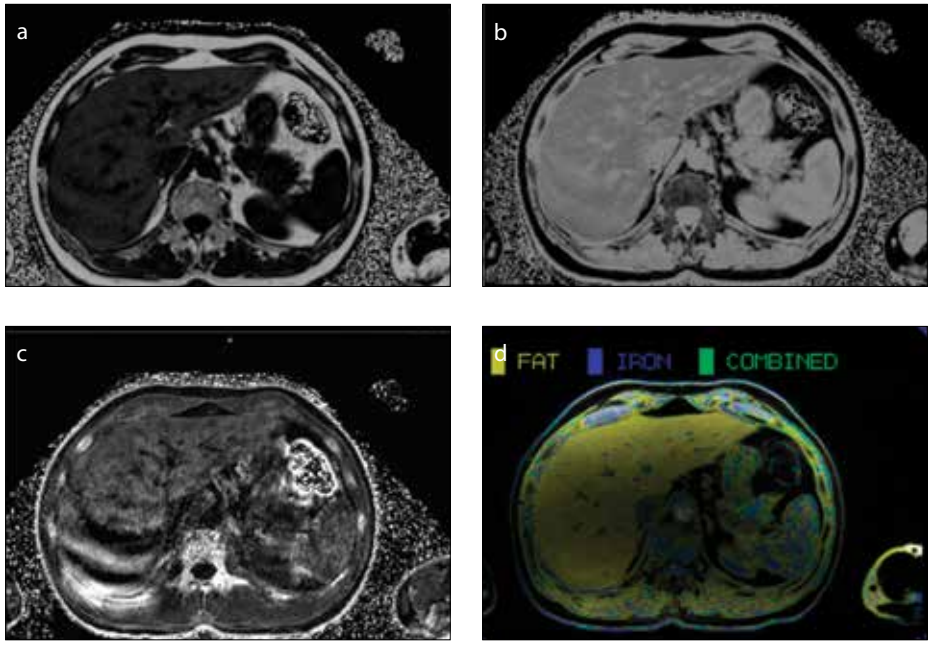

Figure 9. a–d. There is fat accumulation in the liver. Multi-echo Dixon images (a-d).

imaging within a shorter time than Gd-BOPTA. Gd-EOB-DTPA-enhanced MRC enables the detection of biliary injuries by the direct visualization of contrast material extravasation into fluid collections and also by the demonstration of the anatomical site of bile leakage [46, 47].

2.7. MR elastography

Recently, 3D MR elastography has been developed as a technique for assessing the viscoelastic properties of the liver. MR elastography is usually performed with a spin-echo sequence with a time of approximately 20 min. The replacement of the spin-echo sequence by echo-planar sequences has the potential to decrease the acquisition time, which is significant in the radiological applications of MR elastography [48, 49].

2.8. Dixon Sequences and 1H MRS in the Abdomen

Several imaging techniques have been assessed for the evaluation of hepatosteatosis, including US, CT, Dixon-weighted sequences, and proton MRS. Although proton MRS and MRI rely on the signal phase, for example, Dixon techniques have appeared as safe and available tools for evaluating hepatosteatosis, their widespread application is prevented by the time-consuming acquisition process (Figure 9) [50].

3. Breast Imaging

3.1. Contrast-enhanced Mammography and Tomosynthesis

Contrast-enhanced mammography is suitable for the temporal subtraction of images obtained before and after contrast application and the dual energy technique. Skarpathiotakis et al. [51] previously used computer modeling and the processing of contrast-enhanced digital mammography images and found the attainable concentration of a contrast medium detectable with this technique [52].

Tomosynthesis is generally performed by a stationary detector while only the X-ray source moves. As tomosynthesis is performed from different angles, images are acquired without using a grid [53, 54].

4. Cardiac Imaging

4.1. Cardiac MRI with T1 and T2 Mapping

Cardiac MRI has grown over the past several decades into a noninvasive diagnostic imaging tool with a pivotal role in cardiac morphological and functional assessment and tissue characterization. With traditional cardiac MRI examinations, the assessment of various pathologic conditions ranging from ischemic to non-ischemic cardiomyopathy. New T1 and T2 myocardial mapping techniques offer a quantitative assessment of the myocardium using T1 and T2 relaxation times, which may be helpful in focal disease, and demonstrate a special utility in evaluating diffuse myocardial diseases such as edema and fibrosis. By providing a reproducible standard of T1 and T2 values, myocardial mapping may reduce the interpretation variability and error related to subjective analysis and image artifact. T1 and T2 myocardial mapping are quantitative techniques for detecting changes in the myocardial composition. The T2 relaxation time is altered by the water content in the tissue. Myocardial edema has been described in patients with acute myocardial infarction, myocarditis, etc… As with traditional T1 mapping, qualitative T2-weighted imaging is performed with dark-blood turbo spin-echo sequences. The T1 map is a single image that represents a pixel map of the T1 values generated by curve fitting all images in a sequence such as LL, MOLLI, or ShMOLLI. T1 and T2 mapping can have applications in myocardial infarction, cardiomyopathy, myocarditis, thalassemia, amyloidosis, and sarcoidosis (Figure 10) [55-57].

4.2. Dual Energy Cardiac Imaging

Iodine, as a contrast agent, has unique absorption characteristics when penetrated with X-rays of different energy levels. Therefore, iodine mapping shows the myocardial iodine distribution. Dark areas in the iodine map mean that iodine is absent. Dual energy CT is a very fast method, shows cardiac and extra-cardiac pathologies in trauma, has a user-independent modality, and is available in many centers. It has all the benefits of MDCT and many advantages for emergency medical applications (Figure 11) [58].

5. Interventional Radiology

5.1. 3D volume rendering angiography imaging

Despite recent technical innovations, including contrast-enhanced CT, high-resolution CT

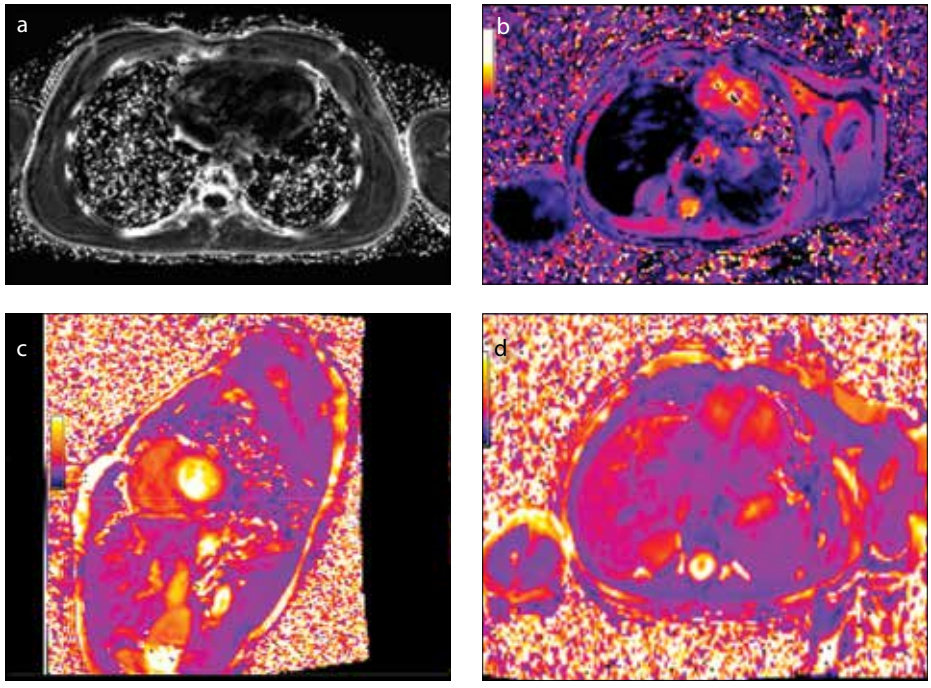

Figure 10. a–d. T1 and T2 mapping images show iron deposition in the heart (a-c) and liver (d).

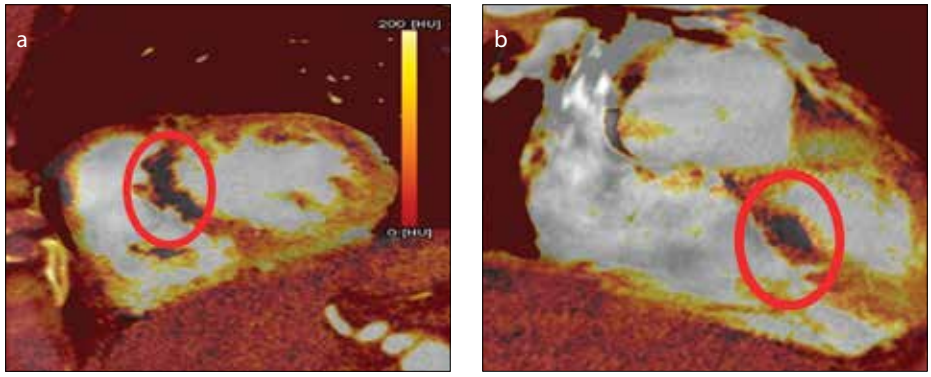

Figure 11. a, b. Myocardial perfusion defects in the dual energy cardiac images (red circles)

Figure 12. a, b. (a) Saccular aneurysm in the 3D volume rendering image (red circles). (b) Saccular aneurysm (red circles) in the maximum intensity projection (MIP) image after DSA.
DSA: digital subtraction angiography

angiography, MR angiography, digital subtraction angiography (DSA) is still thought to be the gold standard for evaluating cerebral aneurysms. Biplane DSA with multiple projections is an efficient technique. 3D DSA images provide valuable information on aneurysmal anatomy, including the relationship with the parent and adjacent vessels (Figure 12). This technique allows fast and safe decision-making regarding the feasibility of endovascular or surgical treatment and provides useful information for performing the chosen treatment. Images are acquired in the 3D rotational DSA mode over an angle of 180°. The run may be performed in one of three different angulations of the C-arm (−30° cranial, 0° axial, or +30° caudal) depending on the orientation of the object of interest [59-61].

5.2. Biopsy-guiding imaging

In recent radiology practice, biopsy-guiding imaging can be performed via US, CT, MRI, PET-CT, and mammography. The preprocedural assessment of biopsy should include consideration of the indication for the procedure and the preprocedural evaluation should include a review of the patient's medical history. Warfarin should be stopped 5–7 days prior to the procedure and may be resumed the day following biopsy. Heparin should be withheld 6–12 h prior to biopsy [62-67].

6. Pediatric Imaging

6.1. Ultra-low-dose Imaging in the Pediatric Population

The largest increase in the use of CT imaging has been in the diagnosis of pediatric disorders. Thorax spiral CT is an imaging method with definitive indications and has a confirmed higher sensitivity and specificity than usual chest radiographies [68]. Evans et al. [69] reported a 40% dose reduction by narrowing the beam collimation from 10 mm to 3 mm with the scan interval kept constant at 10 mm. By reducing the radiation dose of a head CT scan, one can obtain critical diagnostic information, such as trauma and hydrocephalus, needed in a preselected group of pediatric patients. In our radiology department, we use ultra-low-dose CT imaging for evaluating a head CT scan in pediatric trauma patients and detecting a foreign body in the trachea and bronchial tree (Figure 13).

7. Musculoskeletal Imaging

7.1. Arthrography Imaging

MR arthrography of the ankle joint is the preferred imaging technique for evaluating ligamentous damage, osteochondral lesions of the talus, adhesive capsulitis, impingement syndrome, tarsal sinus structures, and loose bodies. At our

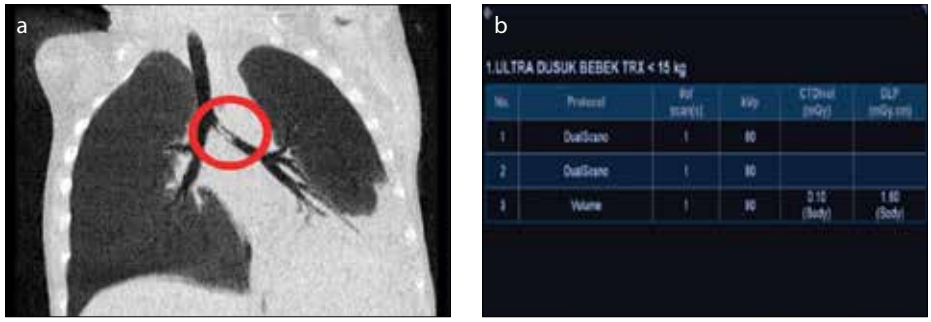

Figure 13. a, b. (a) A foreign body located at the left main bronchus in the ultra-low-dose coronal CT image. (b) Low-dose parameters.

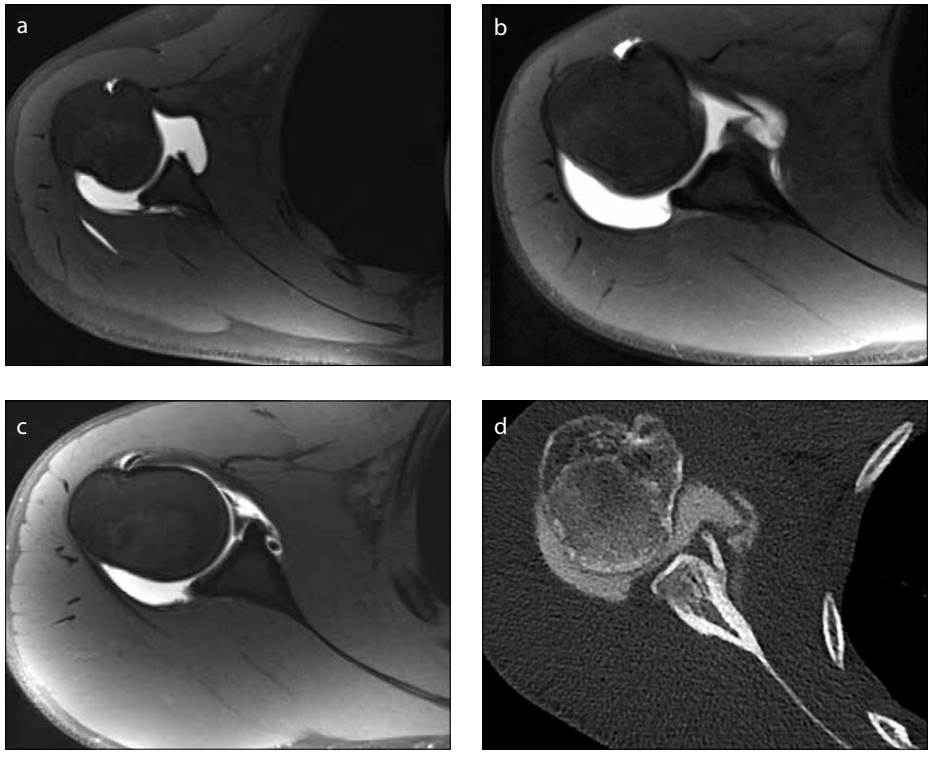

Figure 14. a–d. (a) An anterior labrum periosteal sleeve avulsion lesion on the shoulder MR arthrography. (b-d) A bony Bankart lesion in the shoulder MR and CT arthrography images, respectively. (c) A glenoid labrum articular disruption lesion on shoulder MR arthrography.

institution, we prefer direct MR arthrography for identifying the labroligamentous complex and rotator cuff tendons in the shoulder (Figure 14). In our department, we prepare the diluted contrast medium (0.5 mmol/L gadoterate meglumine, Dotarem, Guerbet, USA) at a concentration of 1:200 (0.1 mL contrast medium diluted in 20 mL normal saline) for the injection procedure. A hemorrhagic effusion is usually an expected complication after dislocation of the glenohumeral joint. The hemorrhage resolves over time, but hemosiderin particles may accumulate in the synovium. These particles are usually not visualized by routine sequences. Concordantly, the VIBE sequence is sensitive and will reveal hemosiderin particles in the synovium and joint space as well as intra-articular air bubbles [70-72].

7.2. 1H Spectroscopy in Musculoskeletal Imaging

MR spectroscopy can be used for noninvasive molecular evaluation. By determining signals of lipids and other metabolites, MRS can reveal information on lesion features and therapy. For example, with phosophorus-31 (31P) MRS, signals from tissue metabolites containing phosphorus are examined, including phosphocreatine, inorganic phosphate, and ATP, which are all metabolites of interest in muscle physiology and diseases. More recently, improved spectral acquisition and analysis techniques, including both single-voxel and MR spectroscopic imaging, along with enhanced gradient performance, have led to the application of proton MRS for the evaluation of musculoskeletal pathology [73, 74].

8. Positron emission tomography-MR Imaging

Positron emission tomography (PET) and MRI might have a high enough diagnostic efficiency to PET-CT for application. Multimodality image fusion has a key role in staging and the evaluation of responses to treatment and surgery. Image registration techniques develop a single fused image in which the functional SPECT or PET image is displayed in color over a grayscale CT or MR image of the same anatomic region. It can reveal a combined functional and molecular imaging evaluation of an extensive diversity of oncological, neurological, and musculoskeletal disorders [75, 76].

9. Further Radiological Imaging Applications

9.1. Silent Scan MRI

Silent scan is a radical neuro-application method that performs the sound of an MRI as silent as a breath. To further the Humanizing MRI commitment, GE Healthcare has introduced many new technologies including the wide bore w Series. The new Silent Scan MRI sequences reveal image quality that is as good as the traditional techniques, but in a way that is much more comfortable for patients. We could perform MRI examinations in many elderly and pediatric patients [77, 78]

9.2. Magnetic Resonance Image Compilation

Magnetic Resonance Image Compilation is a series of standard magnetic resonance weighted images by processing raw data into parametric T1, T2, and PD maps. An operator can change the image contrast by manipulating the time to repetition (TR), time to echo (TE), and inversion time (TI) even after the scan is completed and the patient has exited the MR room [79].

9.3. Frontier Program and 3D Printing

The Frontier Partner Program is looking for startup partners to help us transform manufacturing. Frontier helps entrepreneurs develop their solutions and get them to the market faster, making our industrial customers more competitive. 3D printing is sufficiently simple, reliable, and secure for widespread industrial use. It could accelerate the development of these ideas and get them to market so that our customers can benefit [80].

9.4. Volume Measurement Programs

Volume measurement programs are used to process patient examinations from all modalities in a unified and ergonomic work environment. It is a new-generation workstation for interpreting results and the advanced 3D/4D post processing. It can be adapted to every modality and every organ. It is multipurpose and can be used on a workstation or an application server. It is

also a complete teleradiology station or a specialized station for research work. For example, Myrian® (Intrasense, France) can combine various medical images to extract information [81].

9.5. Computer-aided Detection

Computer-aided detection (CAD) uses pattern recognition software that identifies suspicious findings on the image and brings it to the attention of the radiologist. CAD algorithms search for micro-calcifications and masses on breast mammograms. Current CAD applications include its evaluation of pulmonary densities [82, 83].

Conclusion

New imaging modalities are useful and valuable imaging methods in radiology practice. We recommend that radiologists should be aware of and perform these new imaging modalities.

Peer-review: Externally peer-reviewed.

Author Contributions: Concept - M.K., B.P.; Design - M.K., B.P.; Funding - R.S., M.K.; Materials - S.E., H.O.; Data Collection and/or Processing - A.L., B.P., M.K.; Analysis and/or Interpretation - M.K., B.P., R.S.; Literature review - B.P.; Writing - B.P.; Critical Review - M.K., R.S.

Conflict of Interest: There is no conflict of interest.

Financial Disclosure: There is no any financial disclosure.

References

1. Sanghvi D, Harisinghani M G. Modalities in modern radiology: A synopsis. J Postgrad Med 2010; 56: 85-7. [CrossRef]
2. Ogul H, Bayraktutan U, Kizrak Y, et al. Abdominal Perfusion Computed Tomography. Eurasian J Med 2013; 45: 50-57 [CrossRef]
3. Provenzale JM, Mukundan S, Barboriak DP. Diffusion-weighted and Perfusion MR Imaging for Brain Tumor Characterization and Assessment of Treatment Response. Radiology 2006; 239: 632-49. [CrossRef]
4. Warach S, Dashe JF, Edelman RR. Clinical outcome in ischemic stroke predicted by early diffusion-weighted and perfusion magnetic resonance imaging: preliminary analysis. J Cereb Blood Flow Metab 1996; 16: 53-9. [CrossRef]
5. Sorensen AG, Buonanno FS, Gonzalez RG, et al. Hyperacute stroke: evaluation with combined multi section diffusion weighted and hemodynamically weighted echo-planar MR imaging. Radiology 1996; 199: 391-401. [CrossRef]
6. Alsop DC, Detre JA. Multisection cerebral blood flow MR imaging with continuous arterial spin labeling. Radiology 1998; 208: 410-16. [CrossRef]
7. Sadowski EA, Bennett LK, Chan MR, et al. Nephrogenic systemic fibrosis: risk factors and incidence estimation. Radiology 2007; 243: 148-57. [CrossRef]
8. Yang Y, Frank JA, Hou L, Ye FQ, McLaughlin AC, Duyn JH. Multislice imaging of quantitative cerebral perfusion with pulsed arterial spin labeling. Magn Reson Med 1998; 39: 825-32. [CrossRef]
9. Deibler AR, Pollock JM, Kraft RA, Tan H, Burdette JH, Maldjian JA. Arterial spin-labeling in routine clinical practice, part 1: technique and artifacts. AJNR Am J Neuroradiol 2008; 29: 1228-34. [CrossRef]
10. Tofts PS, Brix G, Buckley DL, et al. Estimating kinetic parameters from dynamic contrast-enhanced T1-weighted MRI of a diffusible tracer: standardized quantities and symbols. J Magn Reson Imaging 1999;10: 223-32. [CrossRef]
11. Gaa J, Warach S, Wen P, Thangaraj V, Wielopolski P, Edelman RR. Noninvasive perfusion imaging of human brain tumors with EPISTAR. Eur Radiol 1996; 6: 518-22. [CrossRef]
12. Ludemann L, Grieger W, Wurm R, et al. Comparison of dynamic contrast-enhanced MRI with WHO tumor grading for gliomas. Eur Radiol 2001; 11: 1231-41. [CrossRef]
13. Norman D, Axel L, Berninger W, et al. Dynamic computed tomography of the brain: techniques, data analysis, and applications. AJR Am J Roentgenol 1981; 136: 759-70. [CrossRef]
14. Axel L. Cerebral blood flow determination by rapid-sequence computed tomography.Radiology 1980; 137: 679-86. [CrossRef]
15. Pierpaoli C, Jezzard P, Basser PJ, Barnett A, Di Chiro G. Diffusion tensor MR imaging of the human brain. Radiology 1996; 201: 637-48. [CrossRef]
16. Jensen JH, Helpern JA, Ramani A, Lu H, Kaczynski K. Diffusional kurtosis imaging: the quantification of non-Gaussian water diffusion by means of magnetic resonance imaging. Magn Reson Med 2005; 53: 1432-40. [CrossRef]
17. Melhem ER, Mori S, Mukundan G, Kraut MA, Pomper MG, van Zijl PC. Diffusion tensor MR imaging of the brain and white matter tractography. AJR Am J Roentgenol 2002; 178: 3-16. [CrossRef]
18. Henson R. Forward inference using functional neuroimaging: dissociations versus associations. Trends Cogn Sci 2006; 10: 64-9. [CrossRef]
19. Poldrack RA. The role of fMRI in cognitive neuroscience: where do we stand?". Curr Opin Neurobiol 2008; 18: 223-7. [CrossRef]
20. Bulakbasi N, Kocaoglu M, Ors F, Tayfun C, Ucoz T. Combination of single voxel proton MR spectroscopy and apparent diffusion coefficient calculation in the evaluation of common brain tumors, AJNR. Am J Neuroradiol 2003; 23: 225-33.
21. Chan YI, Yeung DKW, Leung SF, et al. Proton magnetic resonance spectroscopy of late delayed radiation-induced injury of the brain. J Magn Reson Imaging 1999; 10: 130-7. [CrossRef]
22. Rand SD, Prost R, Li SJ. Proton MR spectroscopy of the brain. Neuroimaging Clin North Am 1999; 9: 379-95.
23. Baker PB, Gillard JH, VanZijji PCM, et al. Acute stroke: evaluation with serial proton MR spectroscopic imaging. Radiology 1994; 192: 723-32. [CrossRef]
24. Schweser F, Deistung A, Lehr BW, et al. Differentiation between diamagnetic and paramagnetic cerebral lesions based on magnetic susceptibility mapping. Med Phys 2010; 37: 5165-78. [CrossRef]
25. Essig M, Waschkies M, Wenz F, et al. Assessment of brain metastases with dynamic susceptibility-weighted contrast-enhanced MR imaging: initial results. Radiology 2003; 228: 193-99. [CrossRef]
26. Battal B, Kocaoglu M, Bulakbasi N et-al. Cerebrospinal fluid flow imaging by using phase-contrast MR technique. Br J Radiol 2011; 84: 758-65. [CrossRef]
27. Ophir J, Cespedes EI, Ponnekanti H, Yazdi Y, Li X. Elastography: a method for imaging the elasticity in biological tissues. Ultrason Imaging 1991; 13: 111-34. [CrossRef]
28. Garra BS, Cespedes EI, Ophir J, Spratt SR, Zuurbier RA, Magnant CM, et al. Elastography of breast lesions: initial clinical results. Radiology 1997; 202: 79-86. [CrossRef]
29. Yu H, Wilson SR. Differentiation of benign from malignant liver masses with Acoustic Radiation Force Impulse technique. Ultrasound Q 2011; 27: 217-23. [CrossRef]
30. Balen FG, Allen CM, Lees WR. Review: ultrasound contrast agents. Clin Radiol 1994;49: 77-82 [CrossRef]
31. Correas JM, Lai X, Qi X, Burns PN. Infusion vs bolus of an ultrasound contrast agent; in vivo dose response measurements of BR1. Invest Radiol 2000; 35:72-79 [CrossRef]
32. Wilson SR, Burns PN, Muradali D, Wilson JA, Xiaoming L. Harmonic hepatic US with microbubble contrast agent: initial experience showing improved characterisation of hemangioma, hepatocellular carcinoma, and metastasis. Radiology 2000; 215: 153-61 [CrossRef]
33. Graser A, Johnson TR, Chandarana H, Macari M. Dual energy CT: preliminary observations and potential clinical applications in the abdomen. Eur Radiol 2009; 19: 13-23. [CrossRef]
34. Johnson TR, Krauss B, Sedlmair M et al. Material differentiation by dual energy CT: initial experience. Eur Radiol 2007; 17: 1510-17. [CrossRef]
35. Macari M, Chandarana H, Schmidt B et al. Abdominal aortic aneurysm: can the arterial phase at CT evaluation after endovascular repair be eliminated to reduce radiation dose? Radiology 2006; 241: 908-14. [CrossRef]
36. Kambadakone AR, Sahani DV. Body perfusion CT: technique, clinical applications, and advances. Radiol Clin North Am 2009; 47: 161-78. [CrossRef]
37. Okada M, Kim T, Murakami T. Hepatocellular nodules in liver cirrhosis: state of the art CT evaluation (perfusion CT/volume helical shuttle scan/dual-energy CT, etc.). Abdom Imaging 2011; 36: 273-81. [CrossRef]
38. Merine D, Takayasu K, Wakao F. Detection of hepatocellular carcinoma: comparison of CT during arterial portography with CT after intraarterial injection of iodized oil. Radiology 1990; 175: 707-10. [CrossRef]
39. Kantarci M, Pirimoglu B, Ozturk G, Aydinli B, Ogul H, Okur A, et al. Clinical utility of hepatic-perfusion computerized tomography in living-donor liver transplantation: a preliminary study. Transplant Proc 2015; 47: 399-407. [CrossRef]
40. Bihan DL, Turner R, Moonen CT, Pekar J. Imaging of diffusion and microcirculation with gradient sensitization: design, strategy, and significance. J Magn Reson Imaging 1991; 1: 7-28 [CrossRef]
41. Turner R, Bihan DL, Chesnick AS. Echo-planar imaging of diffusion and perfusion. Magn Reson Med 1991; 19: 247–253 [CrossRef]
42. Chiu FY, Jao JC, Chen CY, et al. Effect of intravenous gadolinium-DTPA on diffusion-weighted magnetic resonance images for evaluation of focal hepatic lesions. J Comput Assist Tomogr 2005; 29: 176-180 [CrossRef]
43. Chung SR, Lee SS, Kim N, Yu ES, Kim E, Kuhn B, et al. Intravoxel incoherent motion MRI for liver fibrosis assessment: a pilot study. Acta Radiol 2015; 56: 1428-36. [CrossRef]
44. Hagiwara M, Rusinek H, Lee VS, et al. Advanced liver fibrosis: diagnosis with 3D whole-liver perfusion MR imaging initial experience. J Magn Reson Imaging 2003; 18: 372-6.
45. Miyazaki K, Collins D, Walker-Samuel S, et al. Quantitative mapping of hepatic perfusion index

using MR imaging: a potential reproducible tool for assessing tumour response to treatment with the antiangiogenic compound BIBF 1120, a potent triple angiokinase inhibitor. Eur Radiol 2008; 18: 1414-21. [CrossRef]
46. Ogul H, Kantarci M, Pirimoglu B, et al. The efficiency of Gd-EOB-DTPA-enhanced magnetic resonance cholangiography in living donor liver transplantation: a preliminary study. Clin Transplant. 2014; 28: 354-60. [CrossRef]
47. Kantarci M, Pirimoglu B, Ogul H, et al. Can biliary-cyst communication be predicted by Gd-EOB-DTPA-enhanced MR cholangiography before treatment for hepatic hydatid disease? Clin Radiol 2014; 69: 52-8. [CrossRef]
48. Huwart L, Peeters F, Sinkus R, et al. Liver fibrosis: non-invasive assessment with MR elastography. NMR Biomed 2006; 19: 173-9. [CrossRef]
49. Huwart L, Sempoux C, Salameh N et al. Liver fibrosis: noninvasive assessment with MR elastography versus aspartate aminotransferase to-platelet ratio index. Radiology 2007; 245: 458-66. [CrossRef]
50. Bohte AE, vanWerven JR, Bipat S, Stoker J. The diagnostic accuracy of US, CT, MRI and 1H-MRS for the evaluation of hepatic steatosis compared with liver biopsy: a meta-analysis. Eur Radiol 2011; 21: 87-97. [CrossRef]
51. Skarpathiotakis M, Yaffe MJ, Bloomquist AK, et al. Development of contrast digital mammography. Med Phys 2002; 29: 2419-26. [CrossRef]
52. Fischer U, Hermann KP, Baum F. Digital mammography: current state and future aspects. Eur Radiol 2006; 16: 38-44. [CrossRef]
53. Niklason LT, Christian BT, Niklason LE, et al. Digital tomosynthesis in breast imaging. Radiology 1997; 205: 399-406. [CrossRef]
54. Reiser I, Nishikawa RM, Giger ML, et al. Computerized mass detection for digital breast tomosynthesis directly from the projection images. Med Phys 2006; 33: 482-91. [CrossRef]
55. Rogers T, Dabir D, Mahmoud I, et al. Standardization of T1 measurements with MOLLI in differentiation between health and disease: the ConSept study. J Cardiovasc Magn Reson 2013; 15: 78. [CrossRef]
56. Aquaro GD, Positano V, Pingitore A, et al. Quantitative analysis of late gadolinium enhancement in hypertrophic cardiomyopathy. J Cardiovasc Magn Reson 2010; 12: 21 [CrossRef]
57. Kellman P, Aletras AH, Mancini C, McVeigh ER, Arai AE. T2-prepared SSFP improves diagnostic confidence in edema imaging in acute myocardial infarction compared to turbo spin echo. Magn Reson Med 2007; 57: 891-7. [CrossRef]
58. Ruzsics B, Lee H, Zwerner PL, et al. Dual-energy CT of the heart for diagnosing coronary artery stenosis and myocardial ischemia-initial experience. Eur Radiol 2008; 18: 2414-4. [CrossRef]
59. Anxionnat R, Bracard S, et al. 3D Angiography. Clinical interest. First application in interventional neuroradiology. J Neuroradiol. 1998; 25: 251-62.
60. Heautot JF, Chabert E, et al. Analysis of cerebrovascular diseases by a new 3-dimensional computerized X-ray angiography system. Neuroradiology. 1998; 40: 203-9. [CrossRef]
61. Shi WY, Li YD, Li MH, Gu BX, Chen SW, Wang W, Zhang BL, Li M. 3D rotational angiography with volume rendering: The utility in the detection of intracranial aneurysms. Neurol India 2010; 58: 908-13. [CrossRef]
62. Kim C, Erpelding TN, Maslov K, Jankovic L, et al. Handheld array-based photoacoustic probe for guiding needle biopsy of sentinel lymph nodes. J Biomed Opt 2010; 1: 046010. [CrossRef]
63. Caglic I, Breznik S, Matela J, Barrett T. Lesion Targeted CT-Guided Transgluteal Prostate Biopsy in Combination with Prebiopsy MRI in Patients without Rectal Access. Urol Case Rep 2016; 10: 6-8. [CrossRef]
64. Caglic I, Breznik S, Matela J, Barrett T. Lesion Targeted CT-Guided Transgluteal Prostate Biopsy in Combination with Prebiopsy MRI in Patients without Rectal Access. Urol Case Rep 2016; 10: 6-8. [CrossRef]
65. Guo W, Hao B, Chen HJ, et al. PET/CT-guided percutaneous biopsy of FDG-avid metastatic bone lesions in patients with advanced lung cancer: a safe and effective technique. Eur J Nucl Med Mol Imaging 2017; 44: 25-32. [CrossRef]
66. Wang J, Wang X, Liang JW, Gao JD, Bai XF. Clinical application of localized biopsy on breast microcalcification. Zhonghua Wai Ke Za Zhi 2007; 45: 881-2.
67. Dunn AS, Turpie AG. Perioperative management of patients receiving oral anticoagulants: A systematic review. Arch Intern Med 2003; 163: 901-8. [CrossRef]
68. Rothenberg LN, Pentlow KS. Radiation dose in CT. Radiographics 1992; 12: 1225-43. [CrossRef]
69. Evans SH, Davis R, Cooke J, Anderson W. A comparison of radiation doses to the breast in computed tomographic chest examinations for two scanning protocols. Clin Radiol 1989; 40: 45-6. [CrossRef]
70. Ogul H, Guzel Y, Pirimoglu B, et al. The clinical and radiological importance of extraarticular contrast material leakage into adjacent synovial compartments on ankle MR arthrography in patients with OCD and anterolateral impingement. Eur J Radiol 2016; 85: 1857-66. [CrossRef]
71. Ogul H, Karaca L, Can CE, et al. Anatomy, variants, and pathologies of the superior glenohumeral ligament: magnetic resonance imaging with three-dimensional volumetric interpolated breath-hold examination sequence and conventional magnetic resonance arthrography. Korean J Radiol 2014; 15: 508-22. [CrossRef]
72. Ogul H, Kantarci M, Topal M, et al. Extra-articular contrast material leaks into locations unrelated to the injection path in shoulder MR arthrography. Eur Radiol 2014; 24: 2606-13. [CrossRef]
73. Fayad LM, Jacobs MA, Wang X, Carrino JA, Bluemke DA. Musculoskeletal tumors: How to use anatomic, functional, and metabolic MR techniques. Radiology 2012; 265: 340-56.[CrossRef]
74. Subhawong TK, Wang X, Durand DJ, Jacobs MA, Carrino JA, Machado AJ, et al. Proton MR spectroscopy in metabolic assessment of musculoskeletal lesions. AJR Am J Roentgenol 2012; 198: 162-72. [CrossRef]
75. Zaidi H, Mawlawi O, Orton CG. Point / counterpoint. Simultaneous PET/MR will replace PET/CT as the molecular multimodality imaging platform of choice. Med Phys 2007; 34: 1525-8. [CrossRef]
76. Weigert M, Pietrzyk U, Müller S, Palm C, Beyer T. Whole-body PET/CT imaging: combining software- and hardware-based co-registration. Z Med Phys 2008; 18: 59-66. [CrossRef]
77. Alibek S, Vogel M, Sun W, Winkler D, Baker CA, Burke M, Gloger H. Acoustic noise reduction in MRI using Silent Scan: an initial experience. Diagn Interv Radiol 2014; 20: 360-3. [CrossRef]
78. GE Healtcare MR imaging products. www.osha.gov.
79. GE Healtcare MR imaging products. Available from: URL: magic.gehealthcare.com
80. Available from: URL: https://www.frontier.spigit.com/
81. Available from: URL: https://www.imaios.com/
82. Freer TW, Ulissey MJ. Screening mammography with computer-aided detection: prospective study of 12,860 patients in a community breast center. Radiology 2001; 220: 781-6. [CrossRef]
83. Gur D, Sumkin JH, Rockette HE, et al. Changes in breast cancer detection and mammography recall rates after introduction of a computer-aided detection system. J Natl Cancer Inst 2004; 96: 185-90. [CrossRef]